



HAL
open science

Enhancing Stability and Photostability of CsPbI₃ by Reducing Its Dimensionality

Adva Shpatz Dayan, Bat-El Cohen, Sigalit Aharon, Christophe Tenailleau, Malgorzata Wierzbowska, Lioz Etgar

► **To cite this version:**

Adva Shpatz Dayan, Bat-El Cohen, Sigalit Aharon, Christophe Tenailleau, Malgorzata Wierzbowska, et al.. Enhancing Stability and Photostability of CsPbI₃ by Reducing Its Dimensionality. *Chemistry of Materials*, 2018, 30 (21), pp.8017-8024. 10.1021/acs.chemmater.8b03709 . hal-02351004

HAL Id: hal-02351004

<https://hal.science/hal-02351004>

Submitted on 6 Nov 2019

HAL is a multi-disciplinary open access archive for the deposit and dissemination of scientific research documents, whether they are published or not. The documents may come from teaching and research institutions in France or abroad, or from public or private research centers.

L'archive ouverte pluridisciplinaire **HAL**, est destinée au dépôt et à la diffusion de documents scientifiques de niveau recherche, publiés ou non, émanant des établissements d'enseignement et de recherche français ou étrangers, des laboratoires publics ou privés.




Open Archive Toulouse Archive Ouverte (OATAO)

OATAO is an open access repository that collects the work of Toulouse researchers and makes it freely available over the web where possible

This is an author's version published in: <http://oatao.univ-toulouse.fr/24665>


Official URL: <https://doi.org/10.1021/acs.chemmater.8b03709>

To cite this version:

Shpatz Dayan, Adva and Cohen, Bat-El and Aharon, Sigalit and Tenailleau, Christophe  and Wierzbowska, Małgorzata and Etgar, Lioz *Enhancing Stability and Photostability of CsPbI₃ by Reducing Its Dimensionality*. (2018) *Chemistry of Materials*, 30 (21). 8017-8024. ISSN 0897-4756

Any correspondence concerning this service should be sent to the repository administrator: tech-oatao@listes-diff.inp-toulouse.fr

Enhancing Stability and Photostability of CsPbI₃ by Reducing Its Dimensionality

Adva Shpatz Dayan,[†] Bat-El Cohen,[†] Sigalit Aharon,[†] Christophe Tenailleau,[‡] Małgorzata Wierzbowska,[§] and Lioz Etgar^{*,†} 

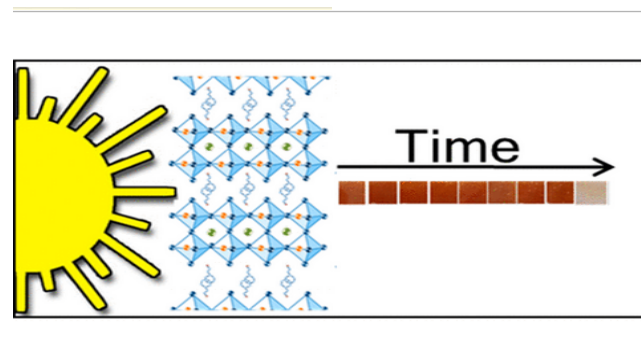
[†]Institute of Chemistry, Casali Center for Applied Chemistry, The Hebrew University of Jerusalem, Jerusalem 91904, Israel

[‡]Laboratoire CIRIMAT, CNRS, INP, UPS, Université de Toulouse, Toulouse 31062, France

[§]Institute of High Pressure Physics, Polish Academy of Sciences, Sokołowska 29/37, 01 142 Warsaw, Poland

Supporting Information

ABSTRACT: Full inorganic perovskites display their potential to function as stable photovoltaic materials better than the hybrid organic–inorganic perovskites. However, to date, the cesium lead iodide perovskite, which displays a promising absorbance range, has suffered from low stability, which degrades to a nonactive photovoltaic phase rapidly. In this work, we show that the black phase of cesium lead iodide can be stabilized when the perovskite dimensionality is reduced. X ray diffraction, absorbance, and scanning electron microscopy were used to follow the degradation process of various dimensionalities under room conditions and 1 sun illumination. When comparing the effect on the stability and photostability of cesium lead iodide with linear or aromatic barrier molecules, the aromatic barrier molecule displays better photostability for over 700 h without degradation under continuous 1 sun illumination than does the linear barrier molecule. Theoretical calculations show that the addition of the barrier molecule makes a different charge distribution over the perovskite structure, which stabilizes the CsPbI₃ black phase. This work provides the possibility to use the CsPbI₃ perovskite as a stable photovoltaic material in solar cells.



INTRODUCTION

Organic–inorganic perovskites have attracted much attention in recent years, especially in the photovoltaic field, owing to their remarkable photophysical properties,^{1–5} such as excellent light capture efficiency, long electron–hole diffusion length, and the possibility to make them from solution.⁶ In the last six years, their power conversion efficiency has approached 23.2%.⁷

One of the most important aspects of a photovoltaic material is the requirement for environmental and photo stability.^{8–14} However, the common perovskite (CH₃NH₃PbI₃) used for solar cells is still far behind in terms of stability, since the organic components are unstable under high temperature and UV radiation conditions.

It was reported that the use of inorganic cations affects the long term stability of perovskite solar cells (PSCs), which remains a major impediment for its industrial application.¹⁵ As a result, there have been several attempts to replace the organic cations with inorganic elements to improve the cells' stability.^{16,17} CsPbI₃ is considered one of the most promising candidates to achieve a stable perovskite structure. The inorganic cation Cs⁺ has a reasonable radius, which provides an appropriate tolerance factor. The Goldschmidt tolerance factor is calculated using the ionic radius of the atoms, which

behave according to the following expression: $t = \frac{r_A + r_X}{\sqrt{2}(r_B + r_X)}$, where r_A is the radius of the A cation, r_B is the radius of the B cation, and r_X is the radius of the anion.

Materials with a tolerance factor of 0.9–1.0 have an ideal cubic structure. The perovskite tends to form an orthorhombic structure when $t < 0.8$ and a cubic structure when $0.8 < t < 1$. More than one crystallographic structure is usually found for perovskite material with a given chemical composition, depending on the temperature and the preparation methods.

CsPbI₃ has a tolerance factor of $t = 0.81$, which suggests that Cs⁺ can stabilize the perovskite structure. However, this value approaches the low limit of the tolerance factor, as mentioned above, due to the radius of Cs⁺ (167 pm),¹⁸ which is almost the smallest size possible that can fit into the octahedral cage. A perovskite film of CsPbI₃ is unstable under room conditions, and it can easily form an orthorhombic yellow phase (δ phase), which is not photovoltaically active.

The symbols α , β , and γ represent the black phases of CsPbI₃ that have photovoltaic activity.¹⁹ To synthesize the black phase, a temperature of over 320 °C is required.^{20–22}

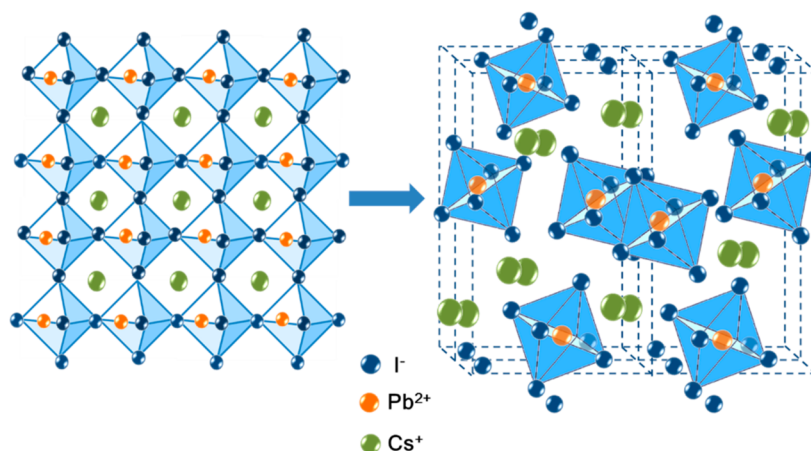


Figure 1. Schematic illustration of the CsPbI₃ in a cubic structure, *Pm3m*, black phase (left). *Pnma*, δ yellow phase (right).

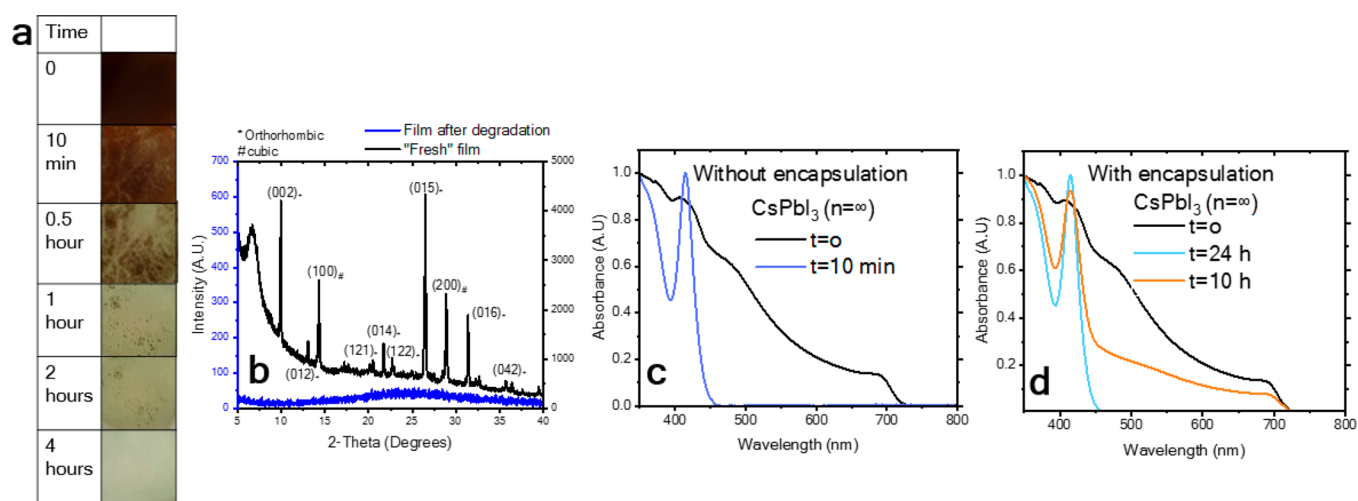


Figure 2. (a) Images of CsPbI₃ film under room conditions (38% humidity, 20 °C) showing the degradation of the film starting from time zero. (b) XRD patterns of CsPbI₃ before and after degradation. The fresh film shows the cubic and orthorhombic structures. (* = orthorhombic, # = cubic) (c) Absorbance spectra for CsPbI₃ film without encapsulation under 1 sun illumination. (d) Absorbance spectra for CsPbI₃ film encapsulated under 1 sun illumination.

Recently it has been reported that the addition of iodic acid (HI) lowers the annealing temperature of CsPbI₃ to 100 °C.²³

Several methods have been studied to achieve the black photovoltaic phase of CsPbI₃, including solvent engineering²³ and halogen exchange.^{24–26} Recently, the concept of low dimensional perovskite has been recognized as a possible route to improve the stability of PSCs.²⁷

The perovskite dimensionality is determined by using a barrier molecule between the inorganic perovskite framework. The barrier molecule is too big to fit into the cage formed by the perovskite octahedra, and therefore, it creates confined inorganic perovskite layers. This low dimensional perovskite creates a quantum well structure, where the inorganic framework and the long organic molecules act as wells and barriers, respectively.

Unlike the three dimensional (3D) perovskite, the low dimensional perovskite has shown promising stability, but it has a much lower power conversion efficiency. The relatively low efficiency of two dimensional (2D) perovskite solar cells (PSCs) is mainly due to the barrier molecules, which could inhibit charge transport through the film. However, it is likely that combining the high efficiency of 3D perovskite with the

enhanced stability of 2D perovskite could be an elegant way to achieve specific requirements from a photovoltaic solar cell.²⁸

In this work, we demonstrate that Cs lead iodide can be stabilized when its dimensionality is reduced using a barrier molecule. We focused on the environmental stability and photostability under continuous illumination and varied humidity of this low dimensional Cs lead iodide perovskite. The differences in stability between a linear barrier molecule (hexylammonium (HA)) and an aromatic barrier molecule (phenylethylammonium (PEA)) were investigated. Absorbance, X ray diffraction (XRD), and scanning electron microscopy (SEM) were used to follow the degradation process. Theoretical calculations predict the way the CsPbI₃ phase is stabilized upon the addition of the barrier molecule and the reason for the different stabilities between the two barriers.

■ RESULTS AND DISCUSSION

At room temperature, CsPbI₃ exhibits the δ yellow phase, which is not photovoltaically active; however, upon annealing, it converts to the black perovskite phase, α CsPbI₃, as the temperature exceeds the transition temperature. The α phase

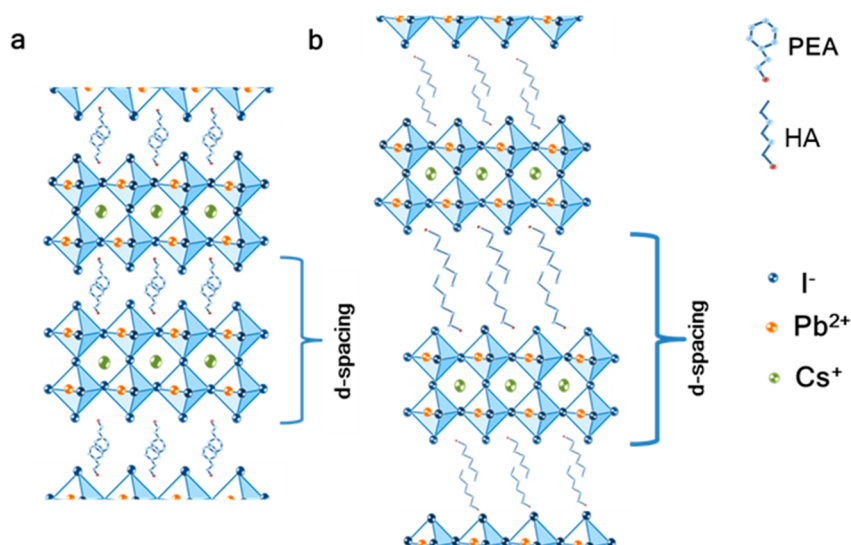


Figure 3. Schematic illustration of both barrier molecules (a) $(\text{PEA})_2\text{Cs}_{n-1}\text{Pb}_n\text{I}_{3n+1}$, where $n = 2$, and (b) $(\text{HA})_2\text{Cs}_{n-1}\text{Pb}_n\text{I}_{3n+1}$, where $n = 2$.

has a cubic structure, with $Pm3m$ symmetry or the 221 space group (based on the International Tables for Crystallography), and it is photovoltaically active. Two other additional phases are tetragonal β CsPbI_3 and orthorhombic γ CsPbI_3 , which are metastable.²⁰ The β phase is also black and has a tetragonal structure. Upon cooling down, the cubic α phase transforms to the β phase with a tetragonal structure. The tetragonal crystal lattice results from stretching a cubic lattice along one of its lattice vectors so that the cube becomes a rectangular prism with a square base and height.

After further cooling of the β phase, a black γ phase is formed with an orthorhombic structure and $Pnmb$ symmetry. The orthorhombic crystal lattice results from stretching a cubic lattice along two of its orthogonal pairs because of two different factors, resulting in a rectangular prism with a rectangular base and height, such that the bases and the height are distinct. All three bases intersect at 90° angles; thus, the three lattice vectors remain mutually orthogonal. The γ phase is still photovoltaically active; however, this is the last stage before it is transformed within minutes, hours, or days, depending on the crystal size and environment to the yellow δ phase, which is not photovoltaically active.³ Figure 1 presents the transition from the black cubic CsPbI_3 structure (α phase) to the δ phase, having a yellow color.

Figure 2b shows the XRD patterns for CsPbI_3 , the orthorhombic (γ) and cubic (α) phases, can be observed in the fresh film. The color of the CsPbI_3 film is black at time zero, as can be seen in Figure 2a. The XRD pattern after degradation is denoted as a blue curve (Figure 2b); no crystallographic peaks are observed (the film is completely amorphous), and the film has a yellow color (all measurements after degradation were taken after leaving the samples for 48 h in a room environment).

Figure 2c,d shows the absorbance of the CsPbI_3 film with and without encapsulation. Without encapsulation, the absorbance loses its shape after 10 min under room conditions (38% humidity, 20°C), whereas with encapsulation the degradation process is inhibited and the film displays a typical absorbance for 10 h under 1 sun illumination. This shows the importance of encapsulated films; however, even with encapsulation, CsPbI_3 is highly sensitive to humidity. Figure 2a presents the CsPbI_3 film (without encapsulation) under

room conditions (38% humidity, 20°C). As can be seen, already after 10 min, degradation can be observed, whereas after 2 and 4 h, the film is completely degraded.

To stabilize the CsPbI_3 structure, we introduced an organic barrier molecule that can form perovskite with a different dimensionality. It was recently shown that the CsPbI_3 structure can be stabilized using an organic barrier. In this work, we studied in detail the stability of low dimensional CsPbI_3 perovskite using linear and aromatic barrier molecules. The low dimensional perovskite (experimental details can be found in the Supporting Information) is based on the chemical formula $(\text{R}-\text{NH}_3)_2\text{Cs}_{n-1}\text{Pb}_n\text{I}_{3n+1}$, where R is the barrier molecule. The stability of the films under room conditions and their photostability under continuous 1 sun illumination, at 30°C and 12% humidity, were studied.

Figure 3 presents two barrier molecules in the two dimensional perovskite structure with CsPbI_3 as the inorganic framework. Usually the inorganic framework consists of methylammonium as the small cation; however, in this case the small cation is Cs^+ . Phenylethylammonium (PEA) is used as the aromatic barrier (Figure 3a) and hexylammonium (HA) as the linear barrier molecule (Figure 3b). These barrier molecules have similar lengths of 9.82 \AA for PEA and 10.03 \AA for HA.²⁹ The aromatic barrier can form a $\pi-\pi$ interaction, which can decrease the d spacing (as denoted in the figure). Using the XRD patterns, the d spacing can be calculated. For example, for $n = 2$ the d spacing of the aromatic barrier is $\sim 14 \text{ \AA}$. However, with the linear barrier molecule (HA) there are van der Waals interactions between the carbon chains; therefore, no overlap is observed between two adjacent barrier molecules, which results in an increase in the d spacing to $\sim 22 \text{ \AA}$ (for $n = 2$).

Figure 4 summarizes the photostability measurements of both barrier molecules (PEA and HA) at different n values (i.e., different dimensionalities). The data in Figure 4 are based on the absorbance spectra presented in Figures 1S and 2S for $n = 2, 4, 6, 8, 40,$ and 60 . The photostability measurements were taken under continuous 1 sun illumination, at 30°C and 12% humidity. Two main conclusions can be drawn from the measurements: (i) the PEA CsPbI_3 perovskite with the aromatic barrier is more stable than the HA CsPbI_3 perovskite with the linear barrier. (ii) Lower n values for perovskite result

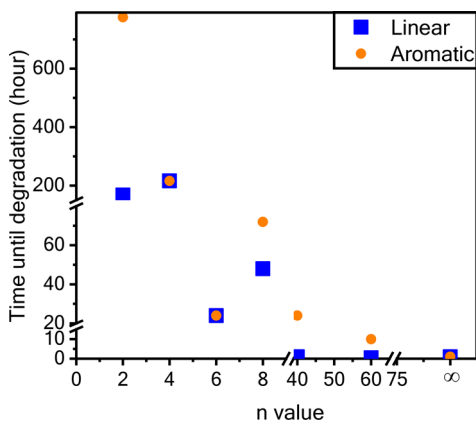


Figure 4. Summary of the photostability measurements under 1 sun illumination, at 30 °C and 12% humidity. The data in this graph are based on the absorbance spectra shown in Figures 1S and 2S.

in better photostability than do higher n values. For example, the aromatic barrier molecule, where $n = 2$ corresponds to $(\text{PEA})_2\text{Cs}_1\text{Pb}_2\text{I}_7$, results in a superior photostability of 720 h under continuous 1 sun illumination, whereas the linear barrier (HA) starts to degrade after 72 h (for $n = 2$). The more barrier molecules that are present in the perovskite structure, the better the stability. The reason for that is based on the fact that the barrier molecule needs to stabilize a smaller number of inorganic octahedron layers in the case of low n values. At $n = 40$ and 60 for both barriers, the film degrades very quickly, but still a difference between the barrier molecules can be observed.

From a theoretical point of view, the effect of both barrier molecules on the stability of the perovskite film is much stronger than the effect of the Cs or methylammonium (MA) cations. This is due to the cation's "strength", which could be measured using electronic space partition techniques such as Mulliken or Löwdin population analysis.

According to these methods, the MA cation is exactly +1, because one electron is given to perovskite, whereas the CsI molecule, used for the synthesis of CsPbI_3 , splits into the +0.725 Cs cation and the negatively charged perovskite. The remaining part of the donor electron, i.e., 0.275, is hybridized with the PbI_3 frame surrounding Cs. This is due to the large overlap of the Cs atomic orbitals with the "molecular" orbitals of the crystal, which is in agreement with the phenomenological model of the Goldschmidt tolerance factor.

Using the same theoretical techniques, we found that the HA and PEA molecules are about +1.5 cations, because the $-\text{NH}_3^+$ donor group is also supported by the $-\text{CH}_2-$ chain embedded in the PbI_3 cluster of the perovskite surface. This additional 0.5 of the electronic wave function, localized at the PbI_3 frame, makes the perovskite film more stable than the bulk crystal. Thus, it proves that low dimensional perovskite films degrade slower than high dimensional perovskite films.

XRD measurements were performed on different 2D and quasi 2D perovskite (different n values) films using the aromatic (PEA) and linear (HA) barrier molecules. The XRD measurements were taken on fresh films (black curves) and on films after degradation (blue curves). Figure 5 shows the perovskite films with PEA as the barrier molecule, and Figure 6 shows perovskite films with HA as the barrier molecule. With PEA, at low n values, i.e., $n = 2, 4,$ and 6 , the 2D peaks in the XRD graphs can be recognized in fresh films,

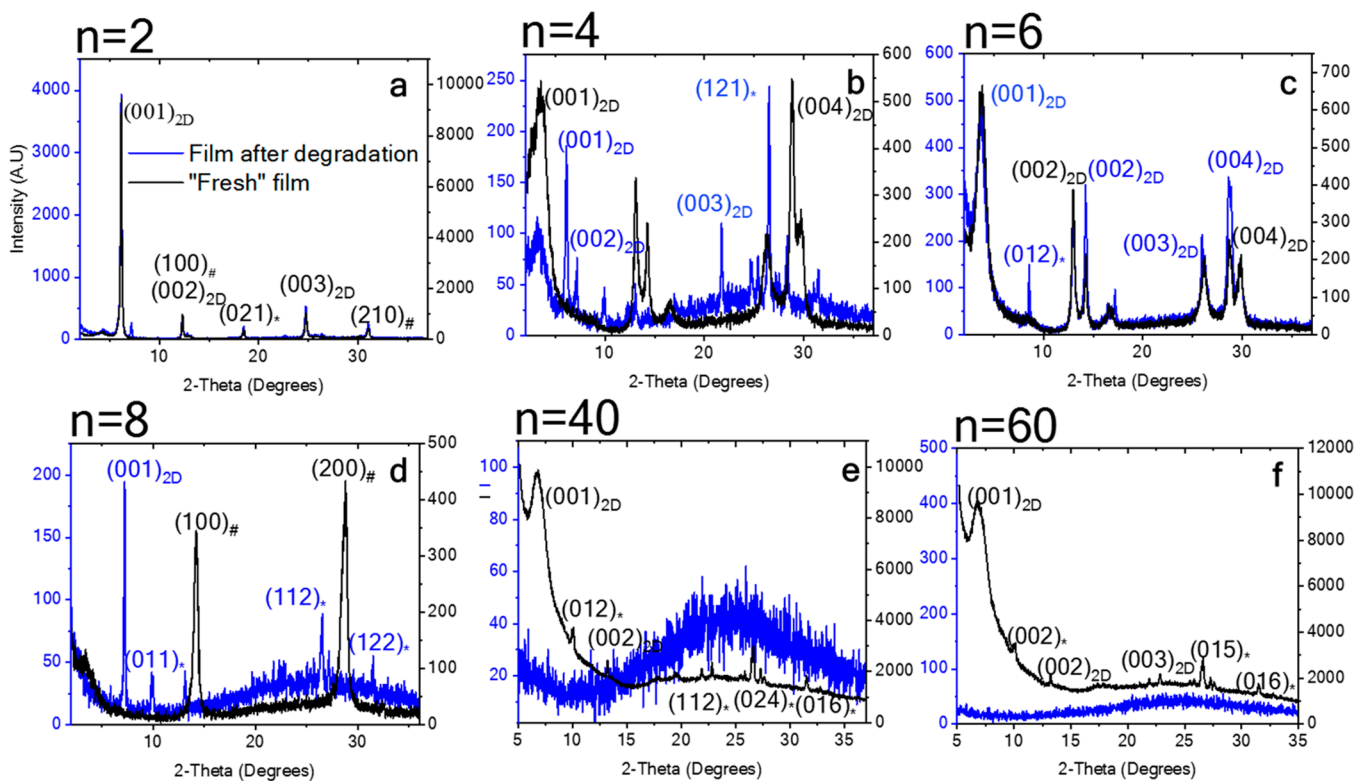


Figure 5. XRD patterns of $(\text{PEA})_2\text{Cs}_{n-1}\text{Pb}_n\text{I}_{3n+1}$ before and after degradation (*=Orthorhombic, # = Cubic). The measurements after degradation were taken after leaving the samples for 48 h at room environment conditions.

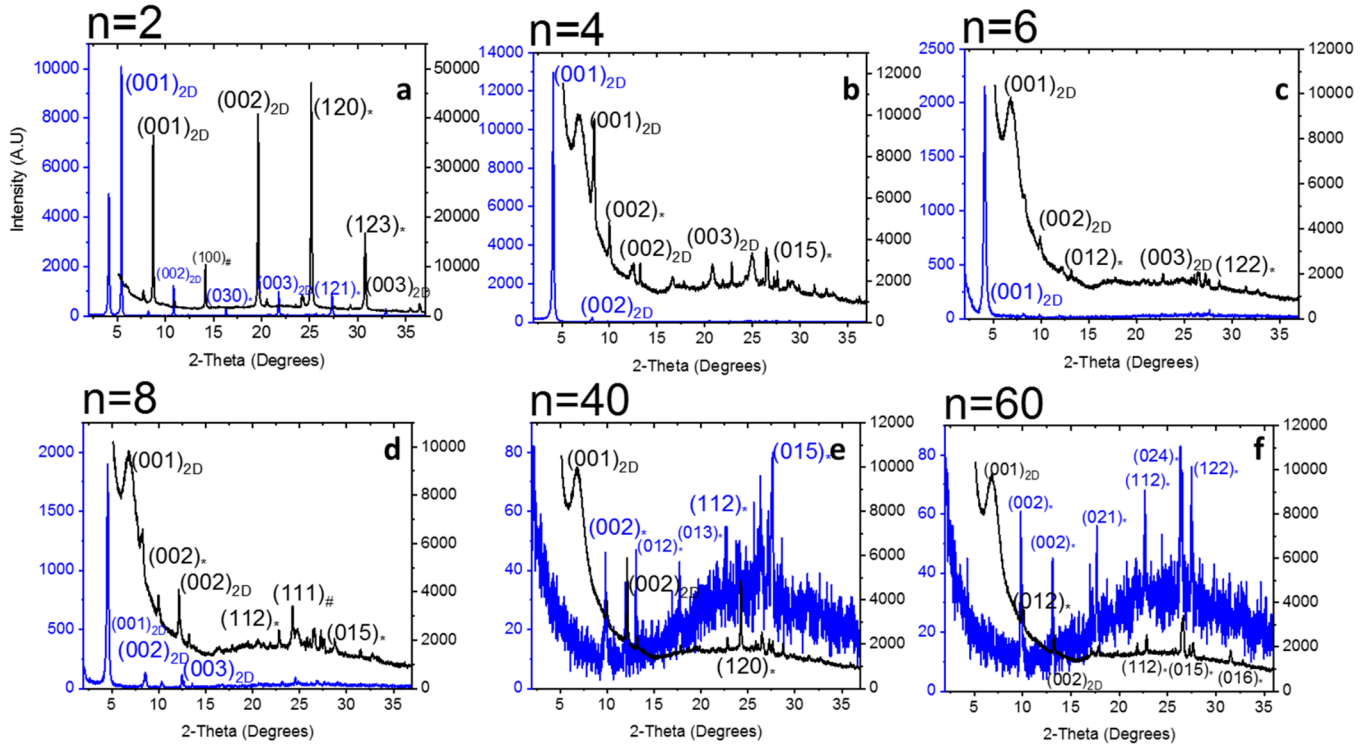


Figure 6. XRD patterns of $(\text{HA})_2\text{Cs}_{n-1}\text{Pb}_n\text{I}_{3n+1}$ before and after degradation. (* = orthorhombic, # = cubic). The measurements after degradation were taken after leaving the samples for 48 h at room environment conditions.

whereas after degradation, some of these peaks disappear but some of them are left over, which indicates the slow degradation process (Figure 5a–c).

In the case of fresh films, where $n = 8, 40,$ and 60 , the 2D peaks can also be observed; however, they are less pronounced than when $n = 2, 4,$ and 6 . After degradation, in contrast to the low n values, where some of the 2D peaks can still be recognized, the high n value films are amorphous (blue curves, Figure 5d–f).

A similar behavior can be observed for the HA barrier molecule, at low n values (i.e., 2, 4, and 6); in the case of fresh films, the 2D peaks can be distinguished clearly, whereas after degradation, fewer peaks can be recognized. With high n values, the same occurs for the HA barrier, as was observed for the PEA barrier, where no peaks can be recognized. Moreover, it can be seen that the intensity of the XRD peaks before degradation was much higher than the intensity after degradation, which indicates better crystallinity.

Figure 7 shows photos of the film degradation with time. The films were without encapsulation and were measured under room environment conditions.

Similarly to the case of photostability, also in this case the low n values indicate better stability (Figure 7a–c, g–i). As indicated, these measurements were performed for films without encapsulation under standard room environment conditions. Therefore, these experiments clearly indicate the resistance of the samples to humidity. Since the amount of the barrier molecule is higher, the perovskite film has better resistance to humidity (i.e., low n values).

The difference between the aromatic versus the linear barrier molecule is observed in this case as well. The aromatic barrier (PEA) displays more enhanced resistance to humidity than does the linear barrier (HA). The color of the PEA film

remains dark brown for a longer time than the film color of the HA barrier molecule.

Interestingly, for high n values where $n = 40$ and $n = 60$, which are very close to the n values of 3D CsPbI_3 perovskite, the film degradation, as a result of humidity, is inhibited compared with 3D CsPbI_3 (see Figure 1a). It appears that even a small amount of a barrier molecule can stabilize the CsPbI_3 black phase against humidity. In addition, in this case the aromatic barrier is a better stabilizer than is the linear barrier.

We can predict this behavior from the theoretical calculations. The destruction of the crystal can be described from the point of view of the defects, which form when the assumed d spacing between the perovskite layers is larger than the optimized distance. The geometries of the perfect perovskite crystal thin films ($n = 2$) with HA and PEA barriers, are described in Table 1. When these systems are stretched out, with a force perpendicular to the perovskite planes, the defects show up on the atomic force conjugate–gradient path. These defects are diverse for the HA and PEA barriers, which are also described in Table 1 as well as in Figure 3S. The linear barrier causes atomic point defects, which seem to pull out iodide atoms from the perovskite surface. Whereas the aromatic barrier causes extended defects, which enlarge the distance between the PbI_2 planes and I–Cs planes. The formation energy of the point defect is twice as high as that of the extended defect, if the crystal calculations with the periodic boundary conditions assume the same geometry in the neighboring unit cells. However, in nature, the appearance of point defects in the measured sample is more seldom than the extended defects. This is due to the lack of defect–defect correlations in the former case. Thus, the total energy necessary to produce in samples the isolated defects, which in nature have the extended character, is actually higher for the PEA barrier. In order to isolate the defects from each

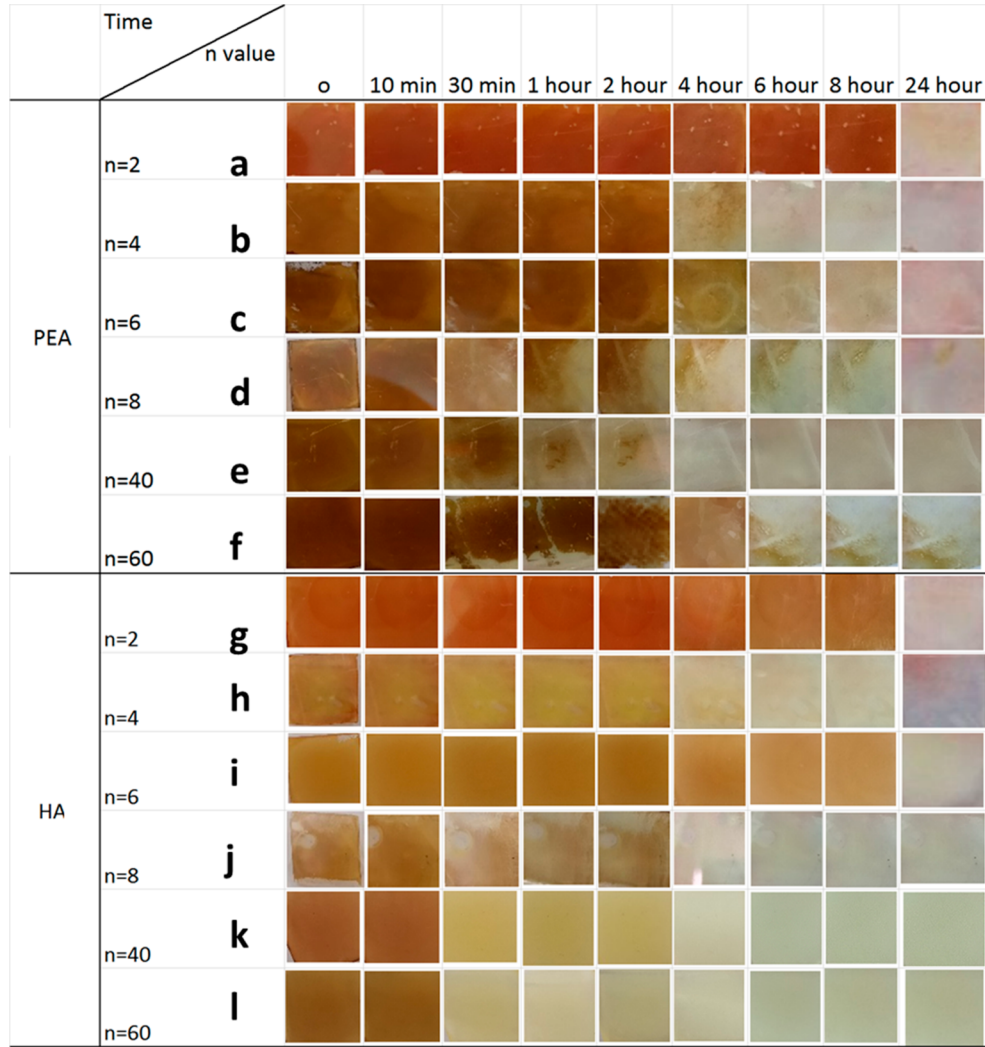


Figure 7. Photos of the different barrier molecules and the various n values under room conditions as a function of time (38% humidity, 20 °C).

Table 1. Interatomic Distances Obtained during the Geometry Optimization Process for the Final (optimized) and Intermediate (defective) Structures^a

case	Pb Pb (film plane) optimized/ distorted	Pb Pb (vertical) optimized/ distorted	Pb I (terminal) optimized/ distorted	defect formation energy
bulk CsPbI ₃	6.288 Å	6.288 Å	3.144 Å	
HA-CsPbI ₃ ($n = 2$)	6.418/6.316 Å	6.530/6.439 Å	3.251/ 3.506 Å	0.405 eV
PEA-CsPbI ₃ ($n = 2$)	6.366/6.275 Å	6.681/7.035 Å	3.141/3.168 Å	0.226 eV

^aThe parameters of the most distorted lattices are denoted in bold.

other, we performed the calculations for the four times larger supercells (in size 2×2) and leaved three cells undefected. The formation energy of the point defect decreased around four times, from 0.45 to 0.113 eV, while the same energy for the extended defect decreased about twice, from 0.226 to 0.093 eV. This is proof that the defects in the samples with PEA tend to cluster because the formation energy does not scale linearly with the system size. Thus, the formation of isolated defects in samples with HA has statistical character and it is adiabatic in time. In contrary, the formation of defects in samples with PEA starts when the energy to form a larger defected cluster is accumulated in the system. This energy, in turn, is proportional to the degradation time. Thus, leading to the higher stability of the films with aromatic barrier than with linear barrier.

Figures 4S and 5S show the average size of the grains after degradation for HA CsPbI₃ and PEA CsPbI₃, respectively. The grain size of HA CsPbI₃ is bigger than that of PEA CsPbI₃ after degradation, and it should be reversely proportional to the number of defective cells in the sample. This size should be larger for point defects in films with HA barriers than for those with PEA barriers. Therefore, it can be assumed that this might be why films with an aromatic barrier (PEA) are more stable, namely, because the formation of extended defects is not an adiabatic process, in contrast to the formation of point defects.

Scanning electron microscopy (SEM) images of the films during degradation for different time lengths under room conditions are presented in Figure 8 for both barrier molecules. Clearly, after degradation, the grains are bigger and have pinholes; in addition, the grain boundaries are becoming

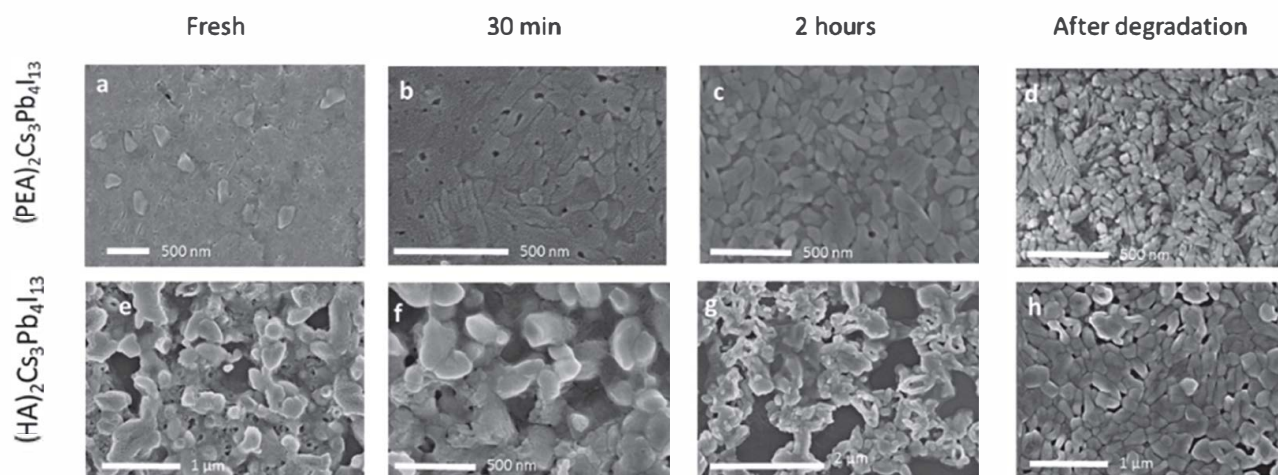


Figure 8. SEM micrographs of fresh films, films after 30 min, 2 h, and films after degradation (48 h), where $n = 4$, for both barrier molecules.

sharper during the degradation process starting from fresh films until films after degradation (48 h). It was reported that the degradation process might start from the grain boundaries, which can explain the SEM images. A similar situation occurred with the linear barrier: the fresh film does not show clear grain boundaries. After 30 min, 2 h, and 48 h under room conditions sharp grain boundaries and pinholes appear. The grain size of the perovskite film after degradation (48 h) with an aromatic barrier is ~ 227 nm in length, and with the linear barrier it is ~ 290 nm in length, as can be seen in Figures 4S and 5S.

CONCLUSIONS

In this work we demonstrated how the black phase of CsPbI_3 can be stabilized when its dimensionality is reduced. Low dimensional CsPbI_3 perovskites were fabricated using two different barrier molecules: linear and aromatic barrier molecules. XRD and SEM show the degradation process of these films, where the low dimensional perovskite, using an aromatic barrier molecule, displays better stability than does the low dimensional perovskite, using a linear barrier molecule. Both barrier molecules display enhanced photostability under continuous 1 sun illumination compared with the 3D CsPbI_3 film, which degrades rapidly. However, the aromatic barrier molecule displays superior photostability compared with the linear barrier. Theoretical calculations explain this observation by the point and extended defects, which increase the time for degradation. Here, we have shown the potential of stabilizing the black phase of CsPbI_3 , which provides the possibility to use it efficiently and stably in PV solar cells.

ASSOCIATED CONTENT

Supporting Information

The Supporting Information is available free of charge on the ACS Publications website at DOI: 10.1021/acs.chemmater.8b03709.

Experimental Section which includes materials and film preparation, absorbance, SEM, size distribution, and theoretical details (PDF)

AUTHOR INFORMATION

Corresponding Author

*(L.E.) E mail: lioz.etgar@mail.huji.ac.il.

ORCID

Lioz Etgar: 0000 0001 6158 8520

Notes

The authors declare no competing financial interest.

ACKNOWLEDGMENTS

We would like to thank the Israel Ministry of Energy and the Israel Science Foundation for their support, Grant Number 2552/17. The calculations were performed using the Prometheus computer in the Cyfronet Supercomputing Centre and supported by the National Science Centre of Poland (the Project No. 2016/23/B/ST8/03480).

REFERENCES

- (1) Kagan, C. R.; Mitzi, D. B.; Dimitrakopoulos, C. D. Organic Inorganic Hybrid Materials as Semiconducting Channels in Thin Film Field Effect Transistors. *Science (Washington, DC, U. S.)* 1999, 286 (5441), 945–947.
- (2) Kim, H. S.; Lee, C. R.; Im, J. H.; Lee, K. B.; Moehl, T.; Marchioro, A.; Moon, S. J.; Humphry Baker, R.; Yum, J. H.; Moser, J. E.; et al. Lead Iodide Perovskite Sensitized All Solid State Submicron Thin Film Mesoscopic Solar Cell with Efficiency Exceeding 9%. *Sci. Rep.* 2012, 2, 591.
- (3) Kojima, A.; Teshima, K.; Shirai, Y.; Miyasaka, T. Organometal Halide Perovskites as Visible Light Sensitizers for Photovoltaic Cells. *J. Am. Chem. Soc.* 2009, 131 (17), 6050–6051.
- (4) Jeon, N. J.; Noh, J. H.; Yang, W. S.; Kim, Y. C.; Ryu, S.; Seo, J.; Seok, S. I. Compositional Engineering of Perovskite Materials for High Performance Solar Cells. *Nature* 2015, 517 (7535), 476–480.
- (5) Etgar, L.; Gao, P.; Xue, Z.; Peng, Q.; Chandiran, A. K.; Liu, B.; Nazeeruddin, M. K.; Grätzel, M. Mesoscopic CH₃NH₃PbI₃/TiO₂ Heterojunction Solar Cells. *J. Am. Chem. Soc.* 2012, 134 (42), 17396–17399.
- (6) Lv, Y.; Guo, Y.; Zhang, H.; Zhou, X.; Chen, H. Enhanced Efficiency and Stability of Fully Air Processed TiO₂ Nanorods Array Based Perovskite Solar Cell Using Commercial Available CuSCN and Carbon. *Sol. Energy* 2018, 173, 7–16.
- (7) Jeon, N. J.; Na, H.; Jung, E. H.; Yang, T. Y.; Lee, Y. G.; Kim, G.; Shin, H. W.; Il Seok, S.; Lee, J.; Seo, J. A Fluorene Terminated Hole Transporting Material for Highly Efficient and Stable Perovskite Solar Cells. *Nat. Energy* 2018, 3, 682–689.
- (8) You, J.; Meng, L.; Song, T. B.; Guo, T. F.; Yang, Y.; Chang, W. H.; Hong, Z.; Chen, H.; Zhou, H.; Chen, Q.; et al. Improved Air Stability of Perovskite Solar Cells via Solution Processed Metal Oxide Transport Layers. *Nat. Nanotechnol.* 2016, 11 (1), 75–81.
- (9) Li, X.; Ibrahim Dar, M.; Yi, C.; Luo, J.; Tschumi, M.; Zakeeruddin, S. M.; Nazeeruddin, M. K.; Han, H.; Grätzel, M.

Improved Performance and Stability of Perovskite Solar Cells by Crystal Crosslinking with Alkylphosphonic Acid ω Ammonium Chlorides. *Nat. Chem.* **2015**, *7* (9), 703–711.

(10) Kaltenbrunner, M.; Adam, G.; Glöwacki, E. D.; Drack, M.; Schwödiauer, R.; Leonat, L.; Apaydin, D. H.; Groiss, H.; Scharber, M. C.; White, M. S.; et al. Flexible High Power per Weight Perovskite Solar Cells with Chromium Oxide Metal Contacts for Improved Stability in Air. *Nat. Mater.* **2015**, *14* (10), 1032–1039.

(11) Han, Y.; Meyer, S.; Dkhissi, Y.; Weber, K.; Pringle, J. M.; Bach, U.; Spiccia, L.; Cheng, Y. B. Degradation Observations of Encapsulated Planar CH₃NH₃PbI₃ Perovskite Solar Cells at High Temperatures and Humidity. *J. Mater. Chem. A* **2015**, *3* (15), 8139–8147.

(12) Smith, I. C.; Hoke, E. T.; Solis Ibarra, D.; McGehee, M. D.; Karunadasa, H. I. A Layered Hybrid Perovskite Solar Cell Absorber with Enhanced Moisture Stability. *Angew. Chem.* **2014**, *126* (42), 11414–11417.

(13) Noh, J. H.; Im, S. H.; Heo, J. H.; Mandal, T. N.; Seok, S. I. Chemical Management for Colorful, Efficient, and Stable Inorganic–Organic Hybrid Nanostructured Solar Cells. *Nano Lett.* **2013**, *13* (4), 1764–1769.

(14) Leijtens, T.; Eperon, G. E.; Pathak, S.; Abate, A.; Lee, M. M.; Snaith, H. J. Overcoming Ultraviolet Light Instability of Sensitized TiO₂ with Meso Superstructured Organometal Tri Halide Perovskite Solar Cells. *Nat. Commun.* **2013**, *4* (1), 2885.

(15) Li, F.; Liu, M. Recent Efficient Strategies for Improving the Moisture Stability of Perovskite Solar Cells. *J. Mater. Chem. A* **2017**, *5* (30), 15447–15459.

(16) Saliba, M.; Matsui, T.; Seo, J. Y.; Domanski, K.; Correa Baena, J. P.; Nazeeruddin, M. K.; Zakeeruddin, S. M.; Tress, W.; Abate, A.; Hagfeldt, A.; et al. Cesium Containing Triple Cation Perovskite Solar Cells: Improved Stability, Reproducibility and High Efficiency. *Energy Environ. Sci.* **2016**, *9* (6), 1989–1997.

(17) Slimi, B.; Mollar, M.; Assaker, I. B.; Kriaa, I.; Chtourou, R.; Mari, B. Perovskite FA₁XMA_xPbI₃ for Solar Cells: Films Formation and Properties. *Energy Procedia* **2016**, *102*, 87–95.

(18) Shannon, R. D. Revised Effective Ionic Radii and Systematic Studies of Interatomic Distances in Halides and Chalcogenides. *Acta Crystallogr., Sect. A: Cryst. Phys., Diffr., Theor. Gen. Crystallogr.* **1976**, *32* (5), 751–767.

(19) Marronnier, A.; Roma, G.; Boyer Richard, S.; Pedesseau, L.; Jancu, J. M.; Bonnassieux, Y.; Katan, C.; Stoumpos, C. C.; Kanatzidis, M. G.; Even, J. Anharmonicity and Disorder in the Black Phases of Cesium Lead Iodide Used for Stable Inorganic Perovskite Solar Cells. *ACS Nano* **2018**, *12* (4), 3477–3486.

(20) Trots, D. M.; Myagkota, S. V. High Temperature Structural Evolution of Caesium and Rubidium Triiodoplumbates. *J. Phys. Chem. Solids* **2008**, *69* (10), 2520–2526.

(21) Akkerman, Q. A.; D’Innocenzo, V.; Accornero, S.; Scarpellini, A.; Petrozza, A.; Prato, M.; Manna, L. Tuning the Optical Properties of Cesium Lead Halide Perovskite Nanocrystals by Anion Exchange Reactions. *J. Am. Chem. Soc.* **2015**, *137* (32), 10276–10281.

(22) Stoumpos, C. C.; Malliakas, C. D.; Kanatzidis, M. G. Semiconducting Tin and Lead Iodide Perovskites with Organic Cations: Phase Transitions, High Mobilities, and Near Infrared Photoluminescent Properties. *Inorg. Chem.* **2013**, *52* (15), 9019–9038.

(23) Eperon, G. E.; Paternò, G. M.; Sutton, R. J.; Zampetti, A.; Haghighirad, A. A.; Cacialli, F.; Snaith, H. J. Inorganic Caesium Lead Iodide Perovskite Solar Cells. *J. Mater. Chem. A* **2015**, *3* (39), 19688–19695.

(24) Luo, P.; Xia, W.; Zhou, S.; Sun, L.; Cheng, J.; Xu, C.; Lu, Y. Solvent Engineering for Ambient Air Processed, Phase Stable CsPbI₃ in Perovskite Solar Cells. *J. Phys. Chem. Lett.* **2016**, *7* (18), 3603–3608.

(25) Beal, R. E.; Slotcavage, D. J.; Leijtens, T.; Bowring, A. R.; Belisle, R. A.; Nguyen, W. H.; Burkhard, G. F.; Hoke, E. T.; McGehee, M. D. Cesium Lead Halide Perovskites with Improved Stability for Tandem Solar Cells. *J. Phys. Chem. Lett.* **2016**, *7* (5), 746–751.

(26) Stoumpos, C. C.; Malliakas, C. D.; Peters, J. A.; Liu, Z.; Sebastian, M.; Im, J.; Chasapis, T. C.; Wibowo, A. C.; Chung, D. Y.; Freeman, A. J.; et al. Crystal Growth of the Perovskite Semiconductor CsPbBr₃: A New Material for High Energy Radiation Detection. *Cryst. Growth Des.* **2013**, *13* (7), 2722–2727.

(27) Cohen, B. E.; Wierzbowska, M.; Etgar, L. High Efficiency and High Open Circuit Voltage in Quasi 2D Perovskite Based Solar Cells. *Adv. Funct. Mater.* **2017**, *27* (5), 1604733.

(28) Grancini, G.; Roldán Carmona, C.; Zimmermann, I.; Mosconi, E.; Lee, X.; Martineau, D.; Narbey, S.; Oswald, F.; De Angelis, F.; Graetzel, M.; et al. One Year Stable Perovskite Solar Cells by 2D/3D Interface Engineering. *Nat. Commun.* **2017**, *8*, 15684.

(29) Muljarov, E. A.; Tikhodeev, S. G.; Gippius, N. A.; Ishihara, T. Excitons in Self Organized Semiconductor/Insulator Superlattices: PbI₂ Based Perovskite Compounds. *Phys. Rev. B: Condens. Matter Phys.* **1995**, *51* (20), 14370–14378.

Supplementary information

Enhancing stability and photostability of CsPbI₃ by reducing its dimensionality

Adva Shpatz Dayan¹, Bat-El Cohen¹, Sigalit Aharon¹, Christophe Tenailleau², Małgorzata Wierzbowska³, and Lioz Etgar^{1*}

¹The Hebrew University of Jerusalem, Institute of Chemistry, Casali Center for Applied Chemistry, Jerusalem, Israel

²Laboratoire CIRIMAT, CNRS, INP, UPS, Université de Toulouse 31062

³Institute of High Pressure Physics, Polish Academy of Sciences, Sokołowska 29/37, 01-142 Warsaw, Poland

* E-mail: lioz.etgar@mail.huji.ac.il

Experimental

Barriers precursor synthesis

PEA

Synthesis of phenylethylammonium iodide (PEAI) was done dropwise: 15 mL of hydroiodic acid (48 wt% in water, Aldrich) into a stirring solution of 10 mL phenylethylamine (99%, Aldrich) dissolved in 10 mL of absolute ethanol at 0 °C. After the addition of acid, the precipitate was left for 20 min at the same temperature. The precipitate was washed three times with diethyl ether and recrystallized twice with ethanol absolute.

HAI

Synthesis of hexylammonium iodide (HAI) was done dropwise: 15 mL of hydroiodic acid (48 wt% in water, Aldrich) into a stirring solution of 10 mL hexylamine (99%, Aldrich) dissolved in 10 mL of ethanol absolute at 0 °C. After the addition of acid, the precipitate was left for 20 min at the same temperature. The precipitate was washed three times with diethyl ether and recrystallized twice with ethanol absolute.

Perovskite Solutions

CsPbI₃ (corresponds for $n = \infty$) solution was prepared by dissolving equivalent amounts of CsI and PbI₂ (Aldrich $\geq 98\%$) in dimethylformamide (DMF) at 0.48 M concentration of each reagent. Quasi 2D perovskite was prepared by dissolving stoichiometric quantity amounts of PEA⁺I⁻ or HAI⁺I⁻, and PbI₂ according to the molecular formula of (PEA)₂Cs_{n-1}PbI_{3n+1} or (HAI)₂Cs_{n-1}PbI_{3n+1} in DMF.

Device Fabrication

Microscope glass was cleaned with ethanol and acetone.

Films characterization

Absorbance spectra were collected with using Jasco V-670 spectrophotometer.

X-ray diffraction measurements were performed with X-ray diffractometer (Tenailleau, Toulouse, France and Uvarov, Jerusalem, Israel)

Uvarov: X-ray powder diffraction measurements were performed in grazing incidence X-ray diffraction (GIXRD) mode on the D8 advance diffractometer (Bruker AXS, Karlsruhe, Germany) with a goniometer radius of 217.5 mm, a secondary graphite monochromator, 2° Soller slits and a 0.2 mm receiving slit. XRD patterns within the range 2° to 60°2θ were recorded at room temperature using CuKα radiation ($\lambda = 1.5418 \text{ \AA}$) with the following measurement conditions: tube voltage of 40 kV, tube current of 40 mA, step-scan mode with a step size of 0.02°2θ and counting time of 1 s-3 s per step. The value of the grazing incidence angle was 2.5°.

Tenailleau: X-ray diffraction (XRD) measurements were performed in nitrogen with a Bruker-AXS D8-ADVANCE instrument in the Bragg-Brentano configuration (with a copper radiation $\text{CuK}\alpha_1 = 1.5405 \text{ \AA}$ and $\text{CuK}\alpha_2 = 1.5445 \text{ \AA}$) that can be equipped with an ANTON-PAAR HTK1200N heating system for in-situ temperature measurements. XRD patterns were recorded from 5 to 40° in 2-Theta with a step scan of 0.014° and 0.3s/step.

Ultra High Resolution Scanning Electron Microscopy (UHR-SEM)

the images were obtained by using Sirion UHR SEM of FEI (Field Emission Instruments), The Netherlands. The measurement conditions were 5 kV at various magnifications, as seen on the data bar of the images (Sigalit would add a little to his instrument and exactly how she did the measurements- how much gold coating)

Extra High-Resolution Scanning Electron Microscopy (XHRSEM)

Magellan XHRSEM was performed using an FEI (Field Emission Instruments), The Netherlands. The measurement conditions were 5 kV.

Theoretical details

The DFT calculations, with the Perdew-Burke-Ernzerhof (PBE) parametrization of the exchange-correlation functional¹, were performed with the pseudopotential based plane-wave Quantum ESPRESSO code². The ultrasoft pseudopotentials³ required the energy cutoff of 30 Ry for the plane waves and 300 Ry for the density. The Broyden-Fletcher-Goldfarb-Shanno algorithm⁴ was used for the geometry optimization until the net force was below $5 \cdot 10^{-3} \text{ eV} \cdot \text{\AA}^{-1}$.

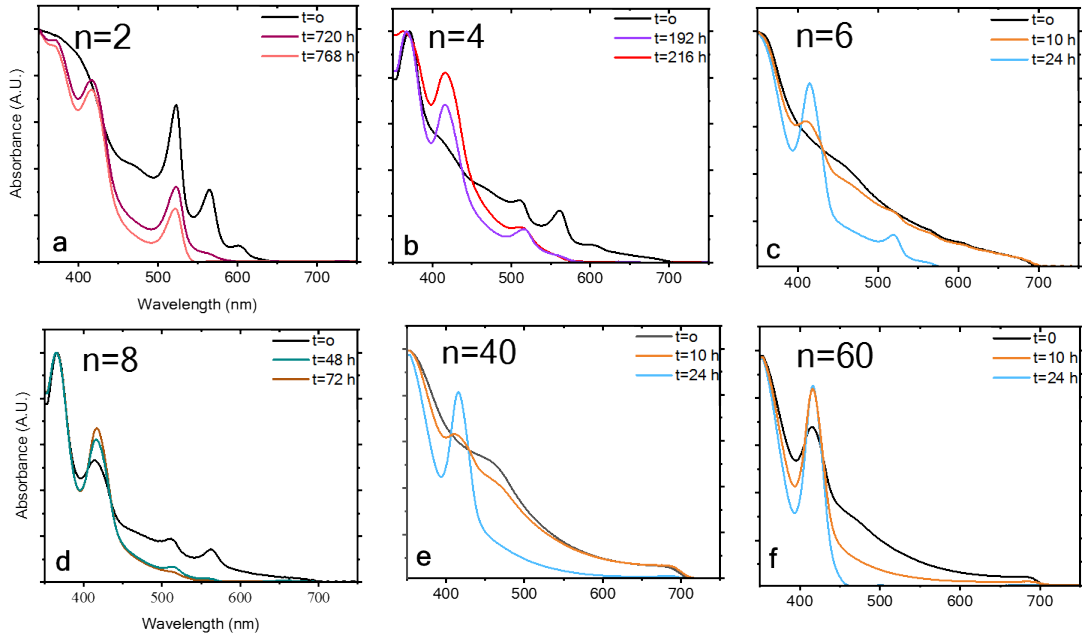


Figure 1S. Normalized absorbance spectra of $(\text{PEA})_2\text{Cs}_{n-1}\text{PbI}_{3n+1}$ under 1 sun illumination with encapsulation.

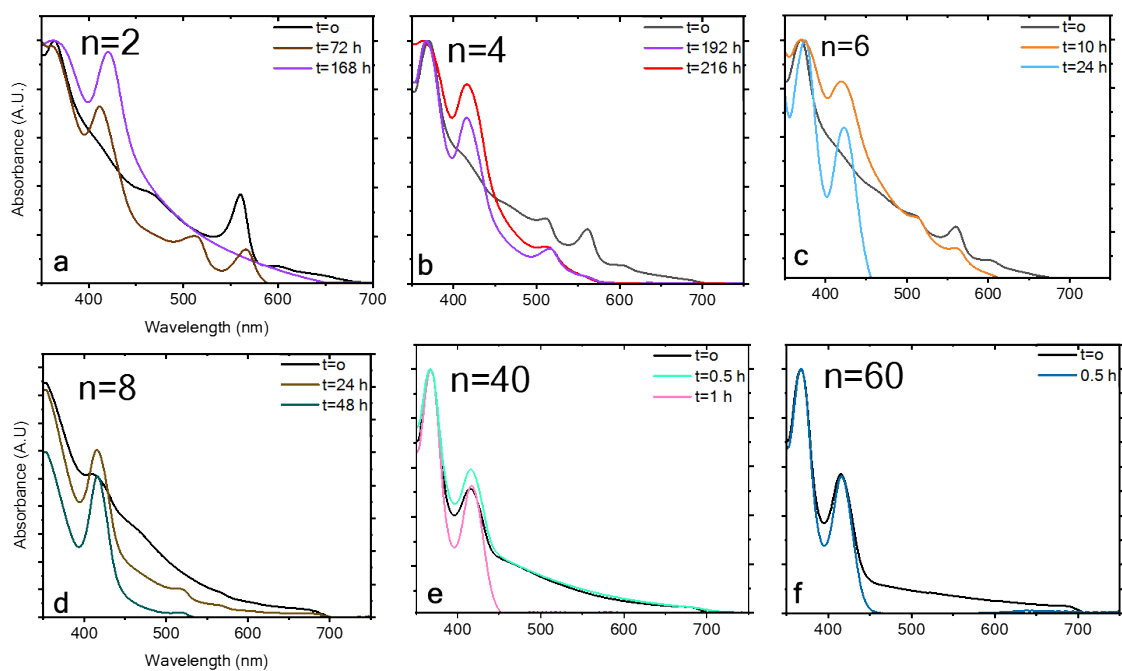


Figure 2S. Normalized absorbance spectra of $(\text{HAI})_2\text{Cs}_{n-1}\text{PbI}_{3n+1}$ under 1 sun illumination with encapsulation.

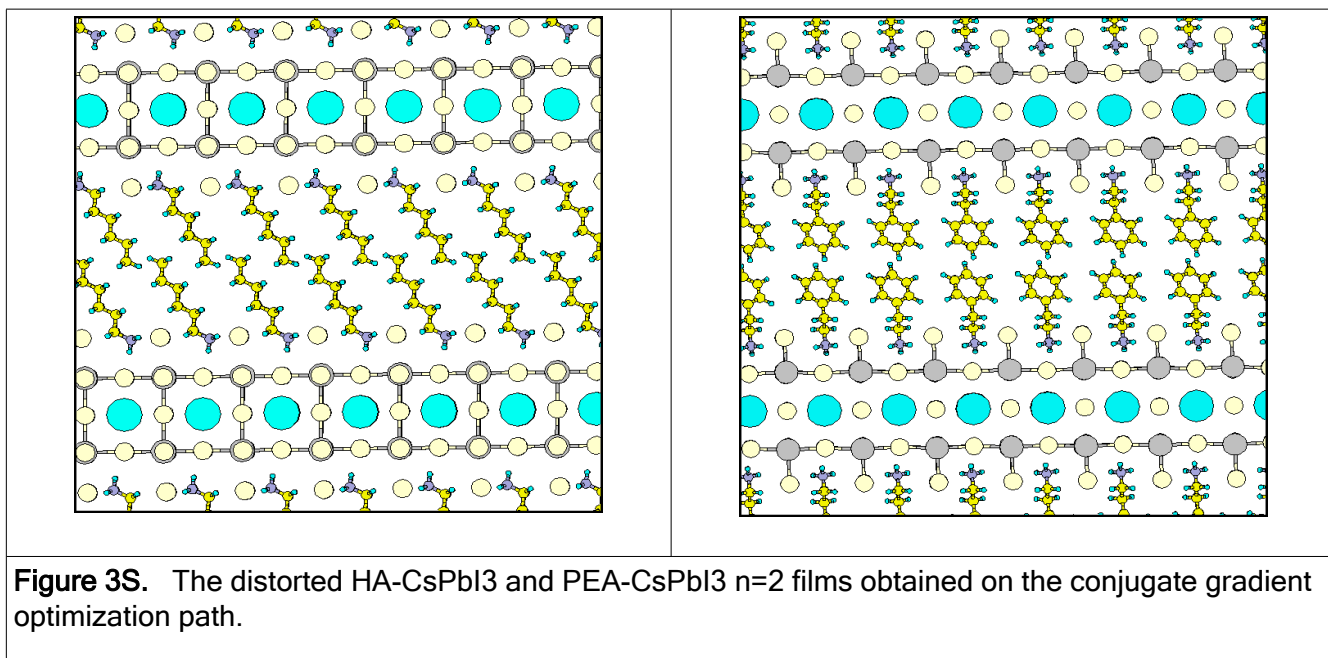


Figure 3S. The distorted HA-CspI3 and PEA-CspI3 $n=2$ films obtained on the conjugate gradient optimization path.

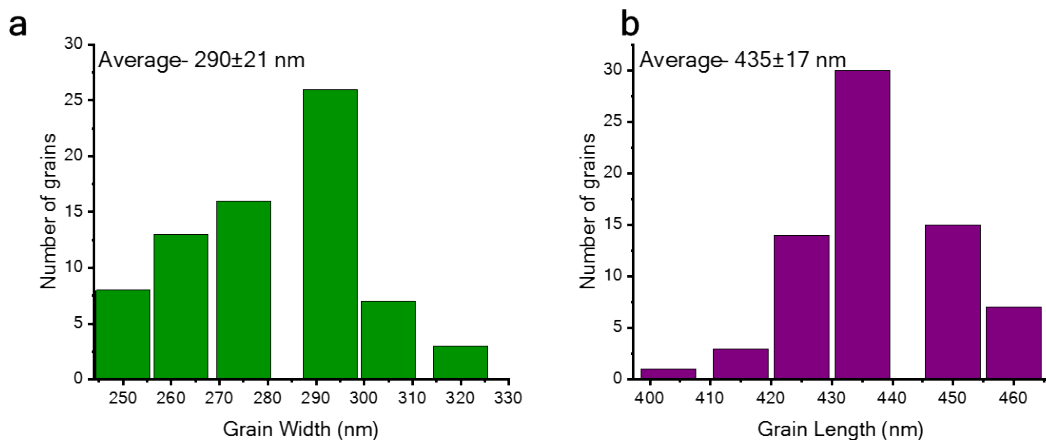


Fig. 4S Histogram of the grain size after degradation of $(\text{HA})_2\text{Cs}_{n-1}\text{PbI}_{3n+1}$

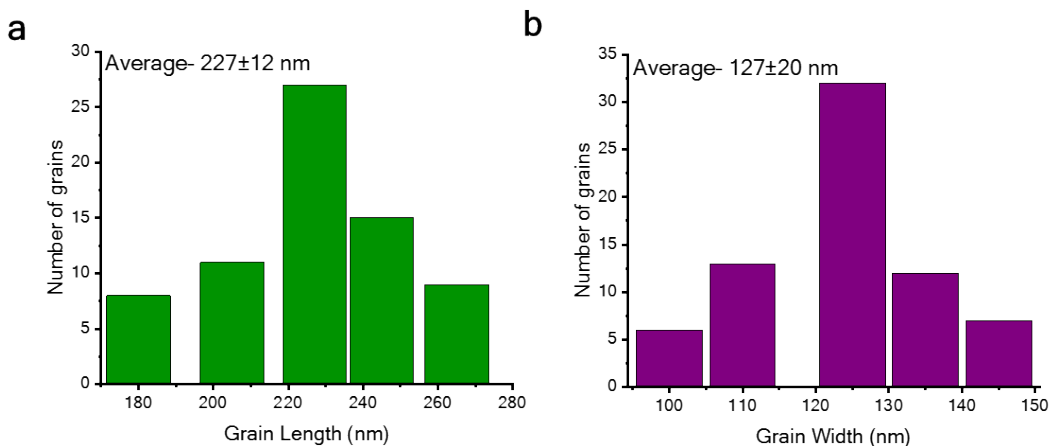


Fig. 5S Histogram of the grain size after degradation of $(\text{PEA})_2\text{Cs}_{n-1}\text{PbI}_{3n+1}$

References

- (1) Perdew, J. P.; Burke, K.; Ernzerhof, M. Generalized Gradient Approximation Made Simple. *Phys. Rev. Lett.* **1996**, *77*(18), 3865-3868.
- (2) Giannozzi, P.; Baroni, S.; Bonini, N.; Calandra, M.; Car, R.; Cavazzoni, C.; Ceresoli, D.; Chiarotti, G. L.; Cococcioni, M.; Dabo, I.; et al. QUANTUM ESPRESSO: A Modular and Open-Source Software Project for Quantum Simulations of Materials. *J. Phys. Condens. Matter* **2009**, *21* (39), 395502.
- (3) Vanderbilt, D. Soft Self-Consistent Pseudopotentials in a Generalized Eigenvalue Formalism. *Phys. Rev. B* **1990**, *41* (11), 7892-7895.
- (4) Fletcher, R. *Practical Methods of Optimization*. 1987, Wiley, 1987.